A composite Mg II index spanning from 1978 to 2003

Rodney A. Viereck,[1] Linton E. Floyd,[2] Patrick C. Crane,[3] Thomas N. Woods,[4] Barry G. Knapp,[4] Gary Rottman,[4] Mark Weber,[5] Lawrence C. Puga,[1] and Matthew T. DeLand[6]

Received 30 March 2004; revised 7 June 2004; accepted 9 August 2004; published 26 October 2004.

[1] The Mg II core-to-wing ratio is a measure of solar chromospheric variability. The Mg II Index, formed by combining various Mg II core-to-wing data sets, has been used in EUV, UV, and total solar irradiance models. It is one of the longest records of solar variability reaching back nearly 25 years. We present a single, continuous time series of the Mg II core-to-wing ratio extending from November 1978 to the present. The Mg II core-to-wing ratio is a measurement that is well suited to the creating of a single time series despite the fact that the seven different instruments measuring the solar flux near 280 nm have different spectral resolutions and sample rates. The Upper Atmosphere Research Satellite (UARS) Solar Ultraviolet Spectral Irradiance Monitor (SUSIM), UARS Solar Stellar Irradiance Comparison Experiment (SOLSTICE), ERS-2/Global Ozone Monitoring Experiment (GOME) and five NOAA solar backscatter ultraviolet data sets were used. Initially, the best data sets were selected to create a time series spanning from 1978 to the present. Then the gaps in the record were filled with data from various other Mg II data sets. Where no alternate data were available, a cubic spline function was used to bridge the missing data. In some cases the data gaps were too long for reasonable spline fits (more than 5 days), and for these gaps the F10.7 cm flux data were scaled to fill the gaps. Thus a continuous, uninterrupted time series of the Mg II core-to-wing ratio was created. The final Mg II time series is compared with other solar activity indices, such as the F10.7, He I 1083, and Sunspot number, to look for trends in the Mg II data. *INDEX TERMS:* 7537 Solar Physics, Astrophysics, and Astronomy: Solar and stellar variability; 7549 Solar Physics, Astrophysics, and Astronomy: Ultraviolet emissions; 7507 Solar Physics, Astrophysics, and Astronomy: Chromosphere; 7536 Solar Physics, Astrophysics, and Astronomy: Solar activity cycle (2162); *KEYWORDS:* solar, variability, Mg II, UV, EUV, ultraviolet

Citation: Viereck, R. A., L. E. Floyd, P. C. Crane, T. N. Woods, B. G. Knapp, G. Rottman, M. Weber, L. C. Puga, and M. T. DeLand (2004), A composite Mg II index spanning from 1978 to 2003, *Space Weather*, *2*, S10005, doi:10.1029/2004SW000084.

1. Introduction

[2] The Mg II core-to-wing ratio has been shown to be a good measure of solar chromospheric activity for solar features and wavelengths that have strong chromospheric components. It has been shown to be a good proxy for solar flux at many EUV wavelengths. In particular, the correlation between the Mg II Index and the integrated solar flux between 25 and 35 nm is extremely good [*Viereck et al.*, 2001]. The Mg II core-to-wing ratio has been found to be a better driver than F10.7 for thermospheric models that calculate satellite drag [*Thuillier and Bruinsma*, 2001; *Rhoden et al.*, 2000] and has been incorporated into empirical spectral models of the solar EUV [*Tobiska et al.*, 2000]. The Mg II index has also been shown to be a good proxy for solar UV irradiances [*Heath and Schlesinger*, 1986; *Donnelly*, 1988] especially near 205 nm [*Cebula et al.*, 1992]. The Mg II index has been used as a proxy for the solar driver in studies of stratospheric ozone and temperatures [e.g., *Hood and Zhou*, 1998] and the Mg II core-to-wing ratio has been used in models of solar UV irradiance as well [*Pap et al.*, 1996; *Lean et al.*, 1997, 2001]. Finally, it has been used as a proxy for the chromospheric component in models of total solar irradiance [*Pap et al.*, 1994; *Lean et al.*, 1997]. On the basis of the Mg II Index and other chromospheric indicators, *Lean et al.* [2001] developed a proxy of solar chromospheric activity going back to 1610 AD. Thus a composite Mg II index (Mg II Index) has significant utility to the scientific community of stratospheric, thermospheric and ionospheric research as well as to total and spectral solar irradiance models relevant to climate change.

[3] In this study, ten Mg II data sets were combined to create a single time series that spans from 1978 to the present. This compilation is unique in that it analyzes all of the available data and determines the best data set for a given period. It then uses the remaining data to fill in data gaps. Each of the contributing data sets has distinctive

[1]Space Environment Center, NOAA, Boulder, Colorado, USA.
[2]Interferometrics, Inc., Chantilly, Virginia, USA.
[3]Naval Research Laboratory, Washington, D. C., USA.
[4]Laboratory for Atmospheric and Space Physics, University of Colorado, Boulder, Colorado, USA.
[5]Institute of Environmental Physics, University of Bremen, Bremen, Germany.
[6]Science Systems and Applications, Inc. (SSAI), Lanham, Maryland, USA.

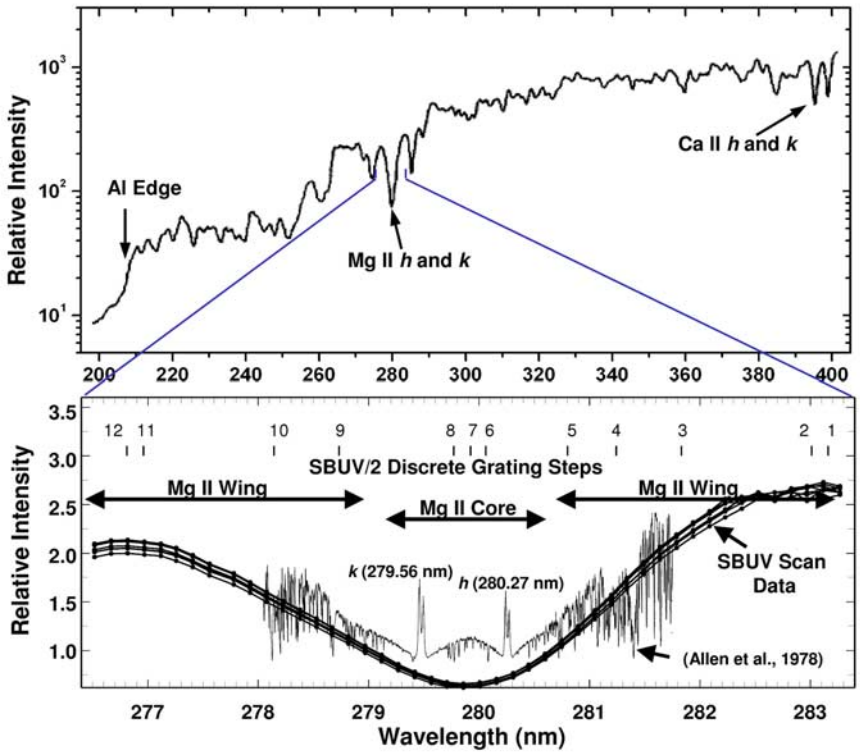

Figure 1. (top) Solar UV spectrum from NOAA 9 SBUV/2 and (bottom) details of the UV spectrum around the Mg II spectral feature at 280 nm. The curves in the bottom plot include a high-resolution spectrum from *Allen et al.* [1978] (thin solid curve), a series of low-resolution spectra from the SBUV (thick curves and dots), and short vertical lines indicating the wavelength positions of the 12 SBUV/2 discrete mode steps. The regions of the spectrum typically defined as core and wing are shown.

features. Some are stable over long periods of time but have more short-period noise. Others have less noise but may drift relative to the average trends. Some of the data sets appear to be good for much of the time that they cover but they may have significant drifts at the beginning or end of the instrument life. All of these factors were considered in compiling this composite index. In spite of the many Mg II data sets, there are periods when no Mg II measurements exist. The short data gaps of less than 5 days are filled with a cubic spline. Longer gaps require that an alternative data set be used. For data gaps of 5 days or longer, the F10.7 cm solar radio flux measurements were scaled to the Mg II index and used to fill the gaps.

[4] In this paper, we review the calculation of the Mg II core-to-wing ratio. Then we present an outline of how the single Mg II Index was created from all of the available data. Details of how this was done are presented in Appendix A. We present estimates of both the short-term and long-term errors and uncertainties in the final Mg II Index. The final Mg II time series is compared with other solar indices such as sunspot number and F10.7 cm flux. Appendix A contains details of the various data sets and how they compared to each other. It also describes in detail how the primary data sets were chosen to define the overall trends in the final time series and how the remaining data were selected and scaled to fill data gaps.

2. Calculating the Mg II Core-to-Wing Ratio

[5] The Mg II core-to-wing ratio is calculated by taking the ratio between the highly variable, chromospheric Mg II *h* and *k* lines at 279.56 and 280.27 nm respectively and the weakly varying photospheric wings. The spectral resolution of the instruments that measure the Mg II vary from 0.1 to 1.1 nm and it is important that the measurement of the photospheric wings be done far enough from the Mg II *h* and *k* lines so as to avoid contamination of the wings by the lines in the core.

[6] Figure 1 shows some of the details of the solar UV spectra near the Mg II absorption/emission feature that are key to these analyses. The top plot shows the full solar spectrum from 250 to 400 nm as measured by the NOAA 9 solar backscatter ultraviolet (SBUV)/2. Several of the relevant features are labeled. The bottom plot in Figure 1 shows the region just around the Mg II features. In this plot there are several curves. There is a

Table 1. Various Mg II Data Sets, Responsible Scientists, and Dates of Coverage

Data Sets	Scientists	Dates
Nimbus7/NOAA 9	Heath, Schlesinger, and Donnelly	7 Nov. 1978 to 28 Feb. 1995
NOAA 9 SBUV/2 VP	Viereck and Puga	31 Dec. 1990 to 18 Feb. 1998
NOAA 9 SBUV/2 DC	DeLand and Cebula	14 March 1985 to 10 April 1997
NOAA 11 SBUV/2 VP	Viereck and Puga	14 Feb. 1989 to 1 Nov. 1992
NOAA 11 SBUV/2 DC	DeLand and Cebula	14 Feb. 1989 to 1 Nov. 1994
EUMTSAT GOME	Weber	27 June 1995 to 31 Dec. 2000
UARS SUSIM	Floyd	12 Oct. 1991 to present
UARS SOLSTICE	de Toma, Knapp, and White	3 Oct. 1991 to 31 Dec. 2000
NOAA 16 SBUV/2	Viereck and Puga	14 Feb 2001 to present
NOAA 17 SBUV/2	Viereck and Puga	2 Oct. 2002 to present

high-resolution curve that clearly resolves the Mg II *h* and *k* lines [*Allen et al.*, 1978]. There are several lower-resolution (1 nm) plots of SBUV data that do not resolve the two Mg II lines. This curve is an example of the SBUV scan mode data. There are twelve positions shown indicating the wavelengths of the twelve steps of the SBUV/2 discrete mode measurements of the Mg II feature. Measurements at these wavelengths are used to calculate the SBUV/2 discrete mode Mg II core-to-wing ratio. Other variable parameters in calculating the SBUV/2 discrete mode Mg II ratios are the specific steps that are used and the electronic ranges that are used. *DeLand and Cebula* [1994] compared various formulations of the Mg II ratios and this discussion will not be repeated here.

[7] There are many other ways that this ratio has been calculated. Data that provides complete spectra can be fit with synthetic spectra and the Mg II line intensities derived from the synthetic spectra that best fits the data. Other instruments (such as the SBUV) may provide only spot measurements at certain wavelengths that can then be used to calculate a ratio. One of the more important consequences of calculating a ratio rather than an absolute value is that it can be quite stable in spite of long-term trends in the overall instrument sensitivity. As long as the change in sensitivity affects the wings as well as the core of the spectral feature, the ratio will insensitive to the instrument changes. Also, for lower-resolution measurements where ratios are calculated rather than spectral fits, it is sometimes important to choose the wavelengths for the wing measurements in places where the spectrum is not changing much with wavelength. In this way, any small variations induced by variable wavelength shifts will be minimal.

[8] Thus it has been shown that the Mg II core-to-wing ratio is a very stable ratio and that in spite of variations between instruments, the various Mg II data sets are linearly correlated to a very high degree. The differences between data sets arise from many factors such as instrument resolution and analysis techniques, however; it appears that as long as the analysis of each of the data sets is consistent, then individual data sets will correlate very well with the other data sets [*Hall and Anderson*, 1988; *de Toma et al.*, 1997; *Cebula and DeLand*, 1998; *White et al.*, 1998]. This property of the Mg II core-to-wing ratio has been used to create long time series from multiple satellites [e.g., *DeLand and Cebula*, 1993; *Donnelly et al.*, 1994; *Viereck and Puga*, 1999].

3. Mg II Index

[9] For this study, ten different Mg II core-to-wing data sets were combined to create the single time series of Mg II data referred to as the Mg II Index. Some of these data are from unique instruments on various NASA and ESA satellites (Solar Ultraviolet Spectral Irradiance Monitor (SUSIM), Solar Stellar Irradiance Comparison Experiment (SOLSTICE), and Global Ozone Monitoring Experiment (GOME)). Other data sets are from a series of similar instruments on multiple satellites (SBUV on NOAA 9, NOAA 11, NOAA 16, NOAA 17). Then there are several different analyses of data from a single instrument. These include the analysis of the NOAA 9 SBUV data by Donnelly, by Viereck and Puga, and by DeLand and Cebula. Similarly the NOAA 11 data were analyzed by different groups. Each of the data sets is described in more detail in Appendix A. They are listed below in Table 1 along with the names of the scientists who created the data sets and the dates of coverage. Each of the data sets and analysis procedure results in a unique range and set of values. Figure 2 shows the original values of the ten Mg II data sets plotted together. The differences are due to various instrument resolutions and analysis techniques. Note that there are both scaling variations and offsets between data sets.

[10] These ten data sets were combined by linearly scaling all of the data to a common scale. Details of the methods used in combing the data are provided in Appendix A. Therefore only an outline of the steps involved will be presented in this section. The linear scaling of Mg II data is quite effective with correlation coefficients between the various data sets ranging from 0.986 to 0.996. Removing suspect data and repeating the scaling process improved the correlations. Rather than simply averaging all of the data to create a single time series, the process chosen here involved selecting key data sets that had the least amount of long-term drift to them. Averaging poorer data with more stable data would have introduces unnecessary secular trends in the final time series. It was also determined that averaging data with data gaps added random noise to the final product associated with the small offsets that were introduced around data gaps and at the start and end of data sets. The four

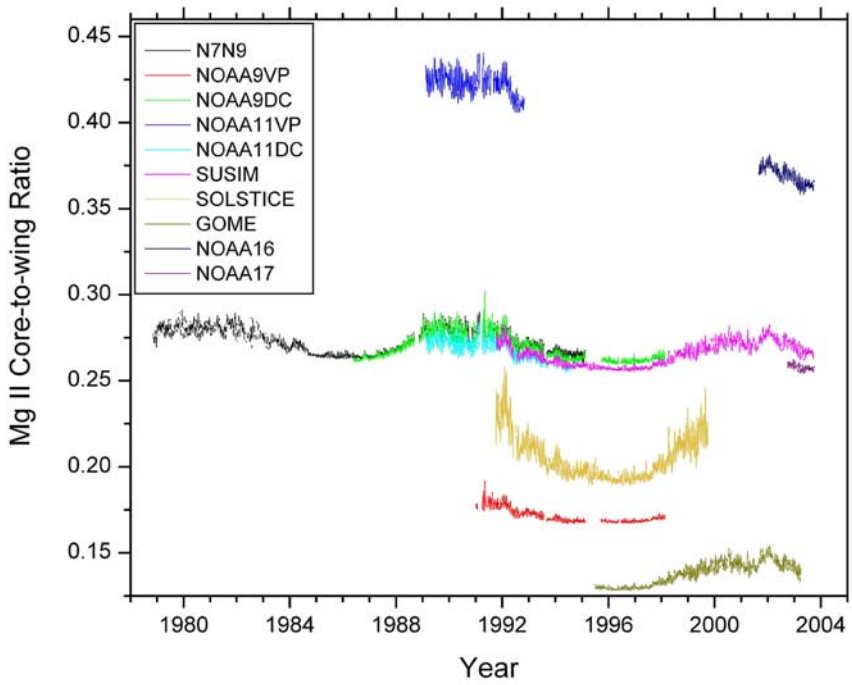

Figure 2. All of the Mg II core-to-wing data sets that contributed to the final time series in this analysis.

primary data sets that defined overall Mg II Index were the Nimbus 7-NOAA 9 SBUV data, the NOAA 9 SBUV VP data, the Upper Atmosphere Research Satellite (UARS) SUSIM data, and the NOAA 16 SBUV data.

[11] Once the overall trends were defined by the four primary data sets, the gaps were filled with the remaining data. In order to avoid small offsets at the endpoints of the data gaps, the secondary data that was selected to fill a particular data gap was corrected slightly by fitting the secondary data around the data gap to the primary data. Then the data points within the data gap were filled. Comparing the various data sets and determining the data sets had the least amount of random and secular noise established a hierarchy of secondary data sets. Even with ten data sets to choose from, there were still gaps after this process was completed. Most of these were 1–3 day gaps during the first 10 years of the 23-year period where only the Nimbus 7/NOAA 9 data set was available. Most of these missing data were filled with a cubic spline. This filled all but two of the remaining data gaps. These last two data gaps were longer than 5 days and the cubic spline method was not able to span the larger data gaps. For these, the F10.7 cm solar radio flux data were scaled and inserted into the Mg II data record. Using these techniques

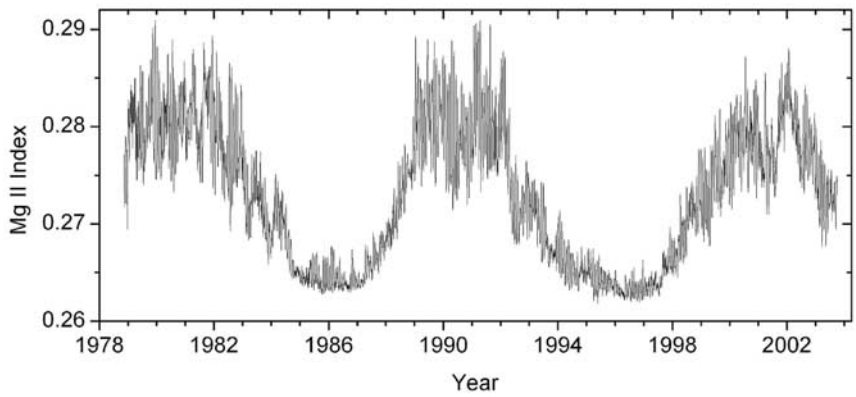

Figure 3. Final time series of the Mg II Index. This is a complete, uninterrupted time series going from November 1978 to the present.

Table 2. Estimated Uncertainties Associated With Each of the Data Sources

Data Sets	Uncertainty, %
N7N9	±0.65
NOAA 9VP	±0.45
NOAA 11VP	±0.50
NOAA 9DC	±0.65
NOAA 11DC	±0.65
SUSIM	±0.50
GOME	±0.60
SOLSTICE	±0.75
NOAA 16	±0.50
NOAA 17	±0.55
F10.7	±1.50
Spline fit	±1.00

all of the gaps in the data set were filled thus creating a single continuous time series of Mg II data. Details on how the data gaps were filled are provided in Appendix A.

[12] This final data set is shown in its entirety in Figure 3. This compilation is unique in two ways. First, it was compiled from all of the available data and this should result in a better final time series. Second, the methods used allowed all the data gaps to be filled, resulting in a continuous time series. It is believed that the process described above and in Appendix A introduces a minimal amount of noise and offsets within the time series. It is hoped that spectral analyses using these data will not have excessive features in the frequency domain that were introduced by the process of combining and scaling the data sets.

[13] There are several features of the Mg II Index, as shown in Figure 3, that should be pointed out. First, the solar cycles 21, 22, and 23 are very obvious and form the largest features in the data. The magnitude of the solar cycle 22 as measured in the Mg II Index are very similar to the magnitude of solar cycle 21 while cycle 23 appears to be a bit smaller than the previous two cycles. This is consistent with other proxies of solar activity such as sunspot number and F10.7 cm flux. On top of the 11-year solar cycle signal is what may appear to be noise but in fact is the 27-day solar rotation signal. These solar rotation modulations have amplitudes near solar maximum that are nearly as large as the solar cycle itself. Neither of these two features is new or surprising.

[14] What may be of most important to many solar research projects and terrestrial climate analyses is the variation from one solar minimum to the next. There have been presentations of total solar irradiance that compare the minimum-minimum values and find marked increases while other analysis show no increase at all. *Wilson* [1997] for instance presented evidence of a substantial increase in the total solar irradiances from cycle 21 to cycle 22 minima. *Fröhlich and Lean* [1998] on the other hand, created a composite index of solar irradiance that had very little increase over the same period. The Mg II data presented here is consistent with the *Fröhlich and Lean* [1998] analysis but there will need to be additional analysis of the total solar irradiance data to determine what the true nature of the sun has been over this period.

4. Uncertainties and Errors

[15] It is important to estimate the uncertainties in these data. The two critical time frames for errors in the data are the short-term random variability and the long-term trends. The data sets used do not include estimates of error. Instead, the scatter in the data was used to estimate the overall uncertainty of the final time series.

[16] To evaluate the scatter or random error, an evaluation was done on the ten Mg II data sets and the F10.7 cm flux. Each data set was compared to the final Mg II Index and was based on the standard deviation of a given data set; an estimate of error is made for that set. The error for a particular data point in the final time series is based on the standard deviation of the data set from which it came.

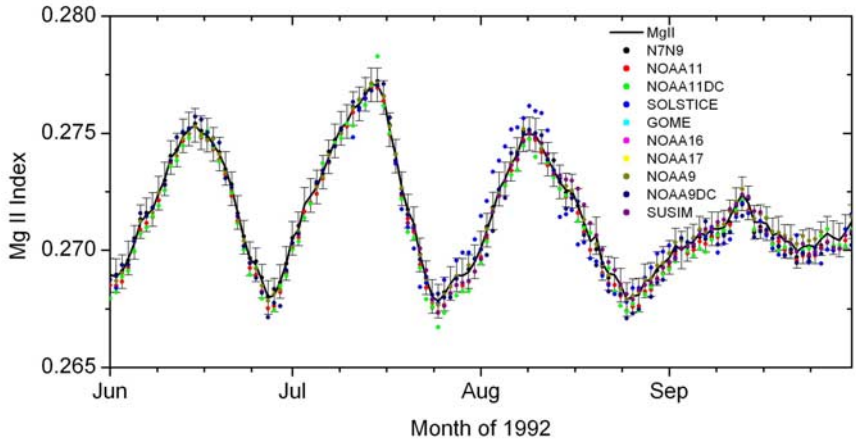

Figure 4. Analysis of the errors during June-September 1992. The error bars capture 90% of the data points. It is therefore expected that the error bars capture the true Mg II Index 90% of the time.

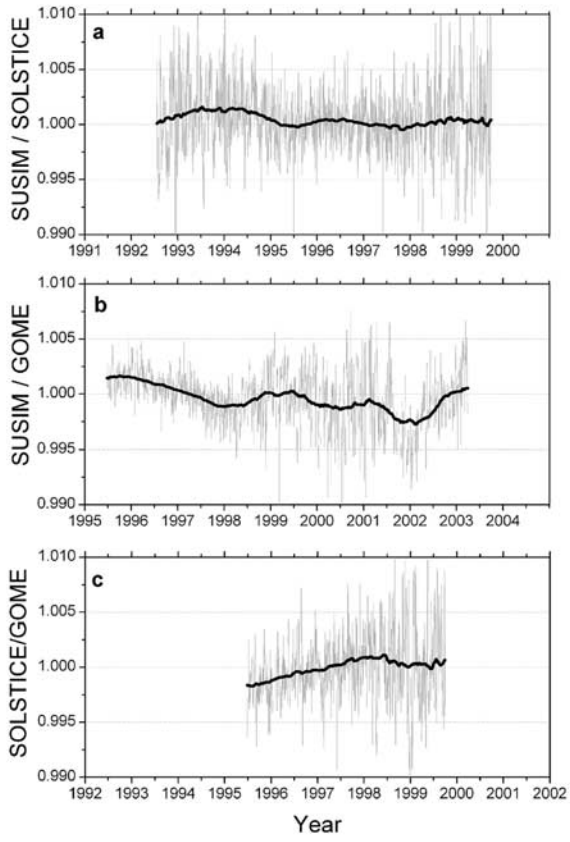

Figure 5. Three ratios of three independent data sets. Both the daily values and 365-day running average are shown. These ratios show that the long-term trends that might exist in any one data set are less than 0.3% per decade.

Similarly, estimates of the uncertainty were established for the data fit with a cubic spline and the F10.7 flux. Table 2 indicates the estimate of the uncertainty for each data set and the spline.

[17] The numbers in this table are such that the error bars capture the true value of the Mg II index for 90% of the data points. Figure 4 shows a 4-month period in 1992. The plot includes the Mg II index from Figure 3 (black curve with error bars) and the various available data sets (colored dots). It is clear from Figure 4 that a majority of the data points fall within the error bars.

[18] With regard to long-term or systematic errors in the Mg II index, there is nothing that provides quantitative estimates. Instead, we rely on the multiple data sets to provide qualitative evidence of the magnitudes of the trends. This of course only works when there are three or more data sets covering the same period. On the basis of this comparison it is probable that the uncertainty in the trends is of the order 0.3% per decade. This can be seen in Figure 5 where the ratios between three independent data sets are shown to typically be less than 0.2% over a decade. Comparisons with other data sets (see next section) confirm that these are reasonable estimates for periods even where there are not multiple data sets for comparison. Trend errors of this magnitude are captured in the errors associated with short-term random variability. Further discussion of the trends in the Mg II is presented in the next section.

5. Comparisons With Other Data Sets

[19] To be useful, the Mg II Index presented here should have long-term trends that reflect only the true nature of the solar chromosphere and no trends related to instrument or analysis errors. These trends are difficult to determine, since it is difficult to separate instrumental trends from actual trends in the data. In an attempt to identify instrument trends, we have compared the Mg II Index to five other long-term solar indices. The five other solar indices are 1) the Mg II Index of Floyd and Crane, 2) the Mg II Index of Viereck and Puga, 3) the F10.7 cm solar radio flux, 4) the daily sunspot number (SSN), and 5) the He I 1083 nm index. The F10.7 and sunspot number are measures of quite different solar phenomena than the Mg II and He I. Thus this comparison is only expected to provide qualitative differences.

[20] Each of these indices was linearly scaled to the Mg II index and then the normalized ratios were derived. Figure 6 shows ratios of the derived Mg II Index over the other solar indices. The ratios have been smoothed with a 365-day running average. The top curve is the Mg II index calculated in this report and is shown as a reference for the phases of the solar cycle.

[21] Since the amplitudes of solar cycles vary, the trends in the data would be most important between solar minima, so we compare the ratios between the two periods of 1985–1987 and 1995–1997. Figure 6 indicates that any trend in the Mg II Index relative to the Mg II Index of Floyd and Crane is minimal. The trend relative to the Mg II Index of Viereck and Puga is downward by about 0.3%. The trends of the Mg II Index relative to both F10.7 and sunspot number decreases by 0.2–0.3%. The trend relative to He I 1083 is more difficult to identify since it exhibits such a strong solar signal, but it appears to have decreased 0.4 to 0.6%.

[22] Relative to these other indices, there may be a slight downward trend in the Mg II Index calculated in this study. However, the magnitude of this trend (0.3%) is similar to the 0.2% per decade uncertainties in the Mg II index as described in the previous sections and so within these uncertainties, the slope between solar minima is essentially zero. On the other hand, since the most recent solar cycle (cycle 23) appears to be lower than the previous two solar cycles, the downward trend may in fact be in the chromospheric emissions rather than an instrumental or analysis effect. It should be noted that SSN and F10.7 reaches a minimum value for some period during solar minimum. So it is possible that the downward trend in Mg II is indeed real and is consistent with the conclusion that it is a better indicator of solar chromospheric activity than either F10.7 or SSN.

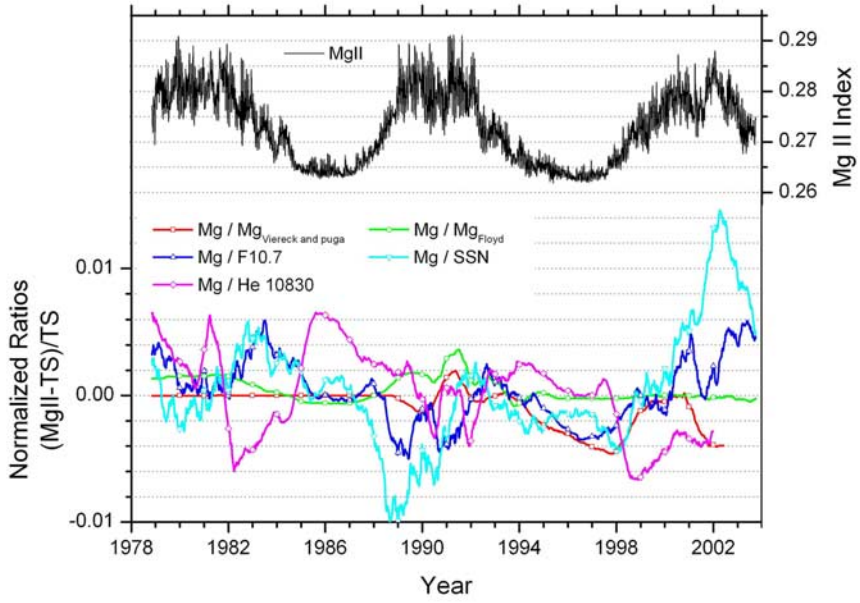

Figure 6. Analysis of the trends in the Mg II Index. The top curve is the Mg II index for reference. The bottom curves are the ratios between the Mg II Index calculated here and other indices. (TS in the label stands for "time series.")

[23] There is an indication of a significant deviation in the ratio between Mg II and the sunspot number near the end of this record. Upon further investigation, it has been determined that this deviation is indeed real and that the sunspot number record is the data set that is unique at the end of 2001 and the beginning of 2002. Comparisons of the SSN with F10.7, solar X-ray flux, EUV flux at 30.4 nm, as well as the Mg II Index all show that while the peak in the monthly averaged sunspot number probably occurred in the spring of 2000, the peak in the monthly averaged values of these other solar indices all show a second and higher peak near the end of 2001 or early in 2002.

6. Summary

[24] The data from ten Mg II core-to-wing data sets have been combined into a single 25-year Mg II Index. The number of data sets and the quality of the data allow the creation of a single time series that captures both the day-to-day variability as well as the long-term trends. The estimate of the error in this Mg II Index is 0.45–1.5% depending on the source of the data. We have shown in this analysis that the correlation between various Mg II data sets is extremely good and that scaling the data to a common scale is quite reasonable. Furthermore, we have selected key data sets to represent the overall trends in the Mg II index. The remaining data are used to fill in short data gaps that exist in the primary data sets. For days when no Mg II data are available, we have used cubic splines and F10.7 cm solar radio flux data to fill data gaps. In this way we have created a continuous uninterrupted record of the Mg II core-to-wing ratio that spans the period from November 1978 to the present. The product of this study is a time series of the Mg II Index covering 25 years, which is available to the community.

[25] The Mg II index clearly shows the rise and fall of the most recent solar cycles. It would appear that the most recent solar maximum levels are not as high as the levels achieved during the previous two maxima despite the second peak seen near the end of 2001 and the beginning of 2002. It should also be noted that the minimum level of the Mg II Index in 1986 is slightly higher than the minimum level in 1997 but the difference is within the uncertainty of the measurements.

[26] A sample of the data file is shown in Table 3. Table 4 shows the source of each data point as listed in the fifth or

Table 3. Sample of the Final ASCII Data File That Contains the Mg II Composite Index[a]

Date	Julian Day	Record Number	Mg II	Source	Uncertainty
19930803	2.449202E6	5384	0.26772	4	8.0E-4
19930804	2.449203E6	5385	0.26747	4	8.0E-4
19930805	2.449204E6	5386	0.2677	10	0.001
19930806	2.449205E6	5387	0.2679	10	0.001
19930807	2.449206E6	5388	0.2680	10	0.001
19930808	2.449207E6	5389	0.2678	12	0.002
19930809	2.449208E6	5390	0.2679	5	0.001
19930810	2.449209E6	5391	0.2688	10	0.001
19930811	2.449210E6	5392	0.26852	4	8.0E-4
19930812	2.449211E6	5393	0.26808	4	8.0E-4

[a]The first column is the date in "yyyymmdd" format. The second column is the Julian day number, where 1 January 2000 is 2.451544E6. The third column is the record number starting at the beginning of the Mg II Index. The fourth column is the Mg II Index. The fifth column is the source of each of the data points (see Table 4). The sixth column is an estimate of the uncertainty.

Table 4. Data Source Associated With Each of the Values in Column 5 of the Mg II Index Data File

Value	Source
1	Nimbus 7/NOAA 9
2	NOAA 9VP
3	NOAA 11VP
4	SUSIM
5	SOLSTICE
6	GOME
7	NOAA 16
8	NOAA 17
9	NOAA 9DC
10	NOAA 11DC
11	F10.7
12	Cubic spline fit

"Source" column of Table 3. These data are available at http://sec.noaa.gov/ftpmenu/sbuv.html in the file "MgII_Index_Version_2004_1.dat."

Appendix A: Details of the Data Sets and Analysis

[27] Details of the data sets and the techniques used in combining them are presented in this Appendix. The process began with choosing the best data sets that provided coverage across the entire time frame. Then these data were linearly scaled to each other thus defining the overall trends of the final time series. Then the data gaps were filled using the remaining data. For periods where no Mg II data were available, cubic splines were used to fill small gaps and the F10.7 cm data were used to fill gaps longer than 5 days.

A1. Data Sets

A1.1. Nimbus and NOAA SBUV Data

[28] The Solar Backscatter Ultraviolet (SBUV and SBUV/2) instruments are designed to measure the stratospheric ozone densities by comparing the backscattered solar spectrum with the observed solar spectrum [*Frederick et al.*, 1986]. In this analysis, we only consider the solar observations. In the spectral scanning mode, the SBUV instruments are capable of observing the solar spectrum from 170 to 400 nm at about 1 nm resolution. In the discrete mode, the grating is moved to specific wavelength positions and longer exposures are taken allowing for better signal-to-noise ratios. Earlier data from Nimbus 7 and NOAA 9 were calculated from the scan mode data. Later data from NOAA 9, NOAA 11, NOAA 16, and NOAA 17 were calculated from discrete mode data since it was found to have less random variability.

[29] The Nimbus 7 SBUV operated from November 1978 to February 1987. The NOAA 9 SBUV instrument operated from 1986 to 1998. The original Mg II core-to-wing ratios were calculated from the Nimbus 7 data by *Heath and Schlesinger* [1986]. *Donnelly et al.* [1994] calculated a similar ratio from the NOAA 9 SBUV using a slightly different formulation and then combined the two data sets to form a continuous time series from November 1978 to the middle of 1994. This data set is referred to in this study as the Nimbus 7/NOAA 9 data set and is considered the reference to which all other data sets will be scaled; however, any of the data sets could have been chosen as the primary data set since the Mg II index is a relative rather than an absolute scale.

[30] In 1994, the NOAA 9 SBUV grating drive started to fail and while the instrument continued to operate until 1998, the standard analysis technique of the discrete mode data that Donnelly used no longer worked well. *Viereck and Puga* [1999] derived an alternate analysis technique for the NOAA 9 Mg II data that reduced the grating drive induced problems. This data set is referred to as the NOAA 9VP (for Viereck and Puga) data and it extends from the end of 1990 to the beginning of 1998 when the NOAA 9 SBUV was turned off. The NOAA 11 data were available from 1989 to 1992. As mentioned above, alternate methods of calculating the Mg II ratio using different grating steps and different electronic ranges is discussed by *Cebula et al.* [1992] and these time series will also be considered here. They are referred to as the NOAA 9DC (for DeLand and Cebula) mode and NOAA 11DC data sets.

[31] SBUV/2 instruments were carried on the NOAA 13 and NOAA 14 spacecraft; however, while the NOAA 13 spacecraft made it into orbit, it failed before the SBUV/2 was turned on. The NOAA 14 SBUV/2 instrument developed grating drive problems early in its life and made too few measurements near the 280 nm Mg II spectral feature to provide useful data for this study.

[32] The next in the series of NOAA spacecraft to carry an SBUV/2 instrument was NOAA 16, which was launched in September of 2000. This instrument has been providing Mg II measurements since February 2001. The NOAA 17 SBUV/2 instrument began operations in October 2002 and is currently providing Mg II measurements.

A1.2. UARS SUSIM and SOLSTICE Data

[33] NASA launched the UARS satellite in September 1991 with SUSIM [*Brueckner et al.*, 1993; *Floyd et al.*, 1998] and SOLSTICE [*Rottman et al.*, 1993; *Woods et al.*, 1993] instruments on board. The SUSIM instrument typically operates with 1.1 nm resolution (similar to the SBUV instruments). The SOLSTICE instrument has a spectral resolution of 0.1 nm. It has been suggested that the higher resolution of SOLSTICE provides measurements of slightly different nature than the other, lower-resolution instruments. Any differences in the data sets may then be physical rather than instrumental [*White et al.*, 1998]. Both of these instruments have provided Mg II data from 1991 to the present although the satellite-operating schedule introduced data gaps near the end of these data sets.

A1.3. GOME Data

[34] The GOME instrument on the European satellite ERS-2 also provided Mg II ratios [*Weber et al.*, 1998]. It has a spectral resolution of about 0.2 nm and was launched in 1995. Like the SOLSTICE instrument, the GOME instru-

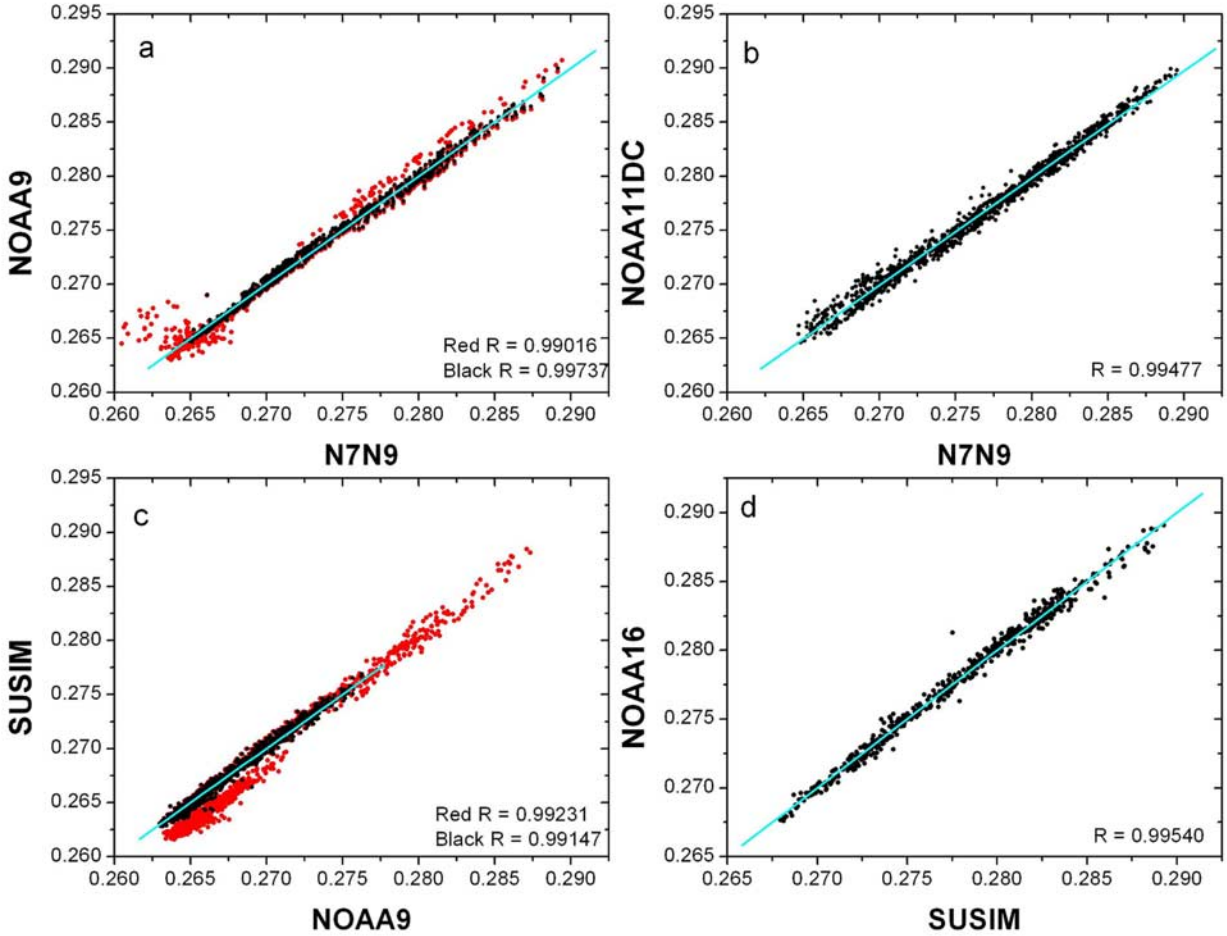

Figure A1. Cross correlations between some of the data sets. The correlation coefficients, *R*, are listed in the corner of each plot. Plots (a) and (c) show both the original data (red dots) and the final data after removing bad data and refitting (black dots). The lines are fits to the black dots.

ment operates with higher spectral resolution than the SBUV and SUSIM instruments. It continues to operate but no longer makes daily Mg II measurements.

A2. Cross Correlations

[35] Comparing various cross correlations illustrates several differences between data sets. Figure A1 shows a few of the more important cross correlations. These plots include the correlation coefficients, *R*, between various data sets. The red dots are the original complete data set and the black dots are the data that remain after removing the bad data (see discussion below). There are several points that can easily be made from Figure A1. First, the data sets are very clearly quite linear in their correlations with *R* ranging from 0.990 to 0.995. In fact similar analysis on the all of the possible cross correlations indicate that the range of values for *R* is from 0.986 to 0.996. Second, there are clear deviations in some of the plots where one of the data sets has had some sort of spurious noise or even a shift from the nominal linear relationship. It is also clear that some data sets have, in general, more noise than others.

[36] It should be noted that the correlation coefficients are strongly dependent on the range of values. Consequently, if the overlap between data sets occurs during the rising or falling phase of the solar cycle where the range of values is relatively large, the coefficients will be higher than if the overlap is at solar minimum where the range of values is small. Large variability increases the correlation coefficients.

[37] In order to better compare and contrast the various data sets, it was necessary to scale each time series to a common scale. This was done by linearly scaling each of them to the Nimbus 7/NOAA 9 data set (referred to as N7N9). For data sets that had little or no overlap with the Nimbus 7/NOAA 9 data set, a secondary data set was used. The selection of secondary data sets was made based on the duration of the overlapping data (where both sets were available) as well as the quality of the secondary data set.

Table A1. Scaling of Data Sets to Secondary Data Sets

Data Set	Secondary Data Set
NOAA 9VP	Nimbus 7/NOAA 9
NOAA 11VP	Nimbus 7/NOAA 9
NOAA 9DC	Nimbus 7/NOAA 9
NOAA 11DC	Nimbus 7/NOAA 9
SUSIM	NOAA 9VP (scaled)
SOLSTICE	NOAA 9VP (scaled)
GOME	SUSIM (scaled)
NOAA 16	SUSIM (scaled)
NOAA 17	SUSIM (scaled)

The data sets and the data sets to which they were scaled are shown in Table A1.

[38] By taking ratios between the scaled data sets, it was possible to identify additional features and, more importantly, any time-dependent drifts or changes in individual data sets. Figure A2 shows the ratios between some of the data sets. It should be noted that the y scale for each of these plots is ±3% indicating that most of the data sets are within ±0.5% of each other. From the plots in Figure A2 and similar plots of other ratios, it is possible to remove some of the problematic data. The ratios from the complete original data sets are shown in red in Figure A2 and the data that is left after removing the bad data is shown in black. If there are three data sets for a given period, and one of the data sets has an offset or trend, then two of the three ratios between these data sets will show this problem allowing the bad data set to be isolated. Using this technique, the bad sections of data were removed as listed in Table A2.

Table A2. Portions of Data Sets Removed

Data Set	Period Removed
Nimbus 7/NOAA 9	7 Sept. 1990 to 26 June 1991
Nimbus 7/NOAA 9	31 March 1994 to end of record
NOAA 9VP	1 July 1995 to end of record
SUSIM	Start of record to 20 July 1992

[39] The black points in Figures A1a and A1c are the remaining good data after removing of the data indicated in Table A2. Note that the correlation coefficients in Figure A1c actually went down after removing the bad data but this is due to the fact that the range of values that are common to both data sets is smaller than in the

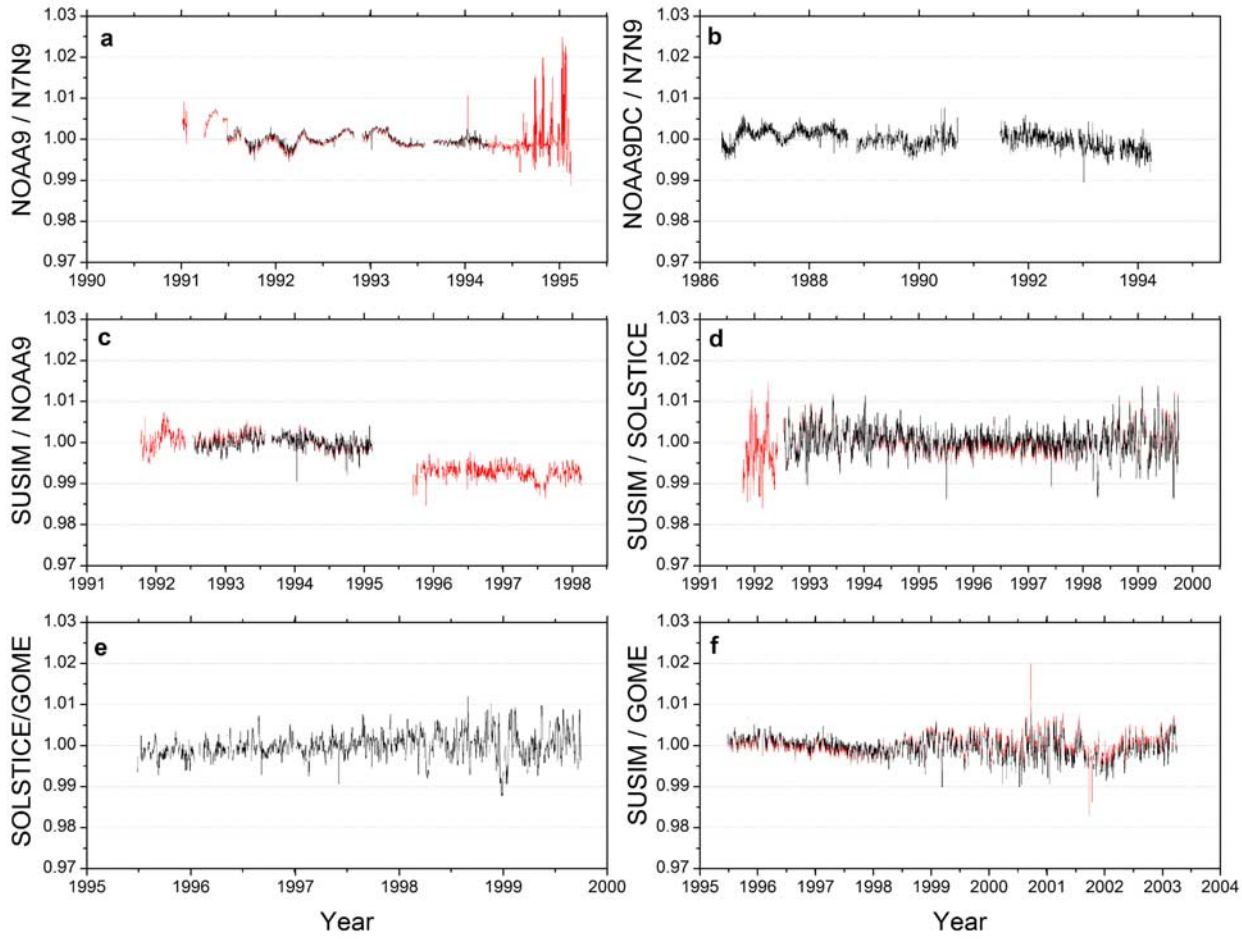

Figure A2. Ratios between various data sets. The red curves are the original data, and the black curves are ratios after removing bad data and refitting the data to the original curves.

Table A3. Primary Data Sets Used to Establish the Overall Features of the Mg II Time Series and the Dates of Coverage

Primary Data	Dates
Nimbus 7/NOAA 9	Nov. 1978 to 14 March 1991
NOAA 9VP	15 March 1991 to 30 Oct. 1992
SUSIM	31 Oct. 1992 to 31 Aug. 2001
NOAA 16	1 Sept. 2001 to present

original data sets. Further analysis indicates that the NOAA 9VP data that were removed were indeed questionable in spite of this lower correlation coefficient.

[40] The curves in Figures A2a, A2c, A2d, and A2f are plots of the original data (red curves) and the final data (black curves) after removal of the bad data and refitting the rescaling data. Figure A2f shows the effect on the long-term trends of removing the bad data. In this plot, none of the data shown were actually removed; however, the removal of other data and the subsequent rescaling of the data in this plot modified the overall trends. From these plots and the many other ratios of the various data sets, the best data sets were selected to use as the primary data for the time series. The Nimbus 7/NOAA 9 data set was the only choice for much of the first half of the period. The NOAA 9VP data were found to have the best overlap with the Nimbus 7/NOAA 9 data and the data sets that follow. In addition, the NOAA 9VP data set has the least amount of random variability and the least amount of long-term trend. Therefore it was selected as the primary data set for the period from early 1991 to late 1992. For similar reasons, the SUSIM data set was selected as primary data set for the period from late 1992 to mid 2001. Since the SUSIM instrument is no longer making continuous daily Mg II values, the NOAA 16 data set was selected as primary for the period from September 2001 to the present. Table A3 lists the primary data sets and the dates of coverage.

[41] These data sets are shown in Figure A3. The overall trend of the Mg II Index, the magnitudes of the three solar cycles, and, the minima between them are all established by these data. To further evaluate the scaling and selection of these four data sets, their overlaps are shown in Figure A4. Note that there is very good agreement and the two curves in each of the three plots in Figure A4 lie on top of each other.

A3. Filling the Data Gaps

[42] There are more than 9000 days in the time series shown in Figure A3, but within this time span there are approximately 1300 days missing from the original primary data sets. Most of these are small 1–3 day gaps, especially in the Nimbus 7/NOAA 9 data set. The gaps were filled three ways. The first method was to use other Mg II data sets when available. This worked well for the second half of the period where multiple instruments were monitoring the Mg II region of the spectrum. The second method of filling gaps was to use a cubic spline fit to fill gaps of less than 5 days. This was required for the early part of the data record where only one data set was available. After applying these two methods, there were still several data gaps of longer than 5 days. For these data points, the missing data were filled with a scaled version of the F10.7 cm solar radio flux. It should be noted that an alternative to the F10.7 cm flux might be the He I 1083 nm equivalent width proxy which is more appropriate as a chromospheric proxy than

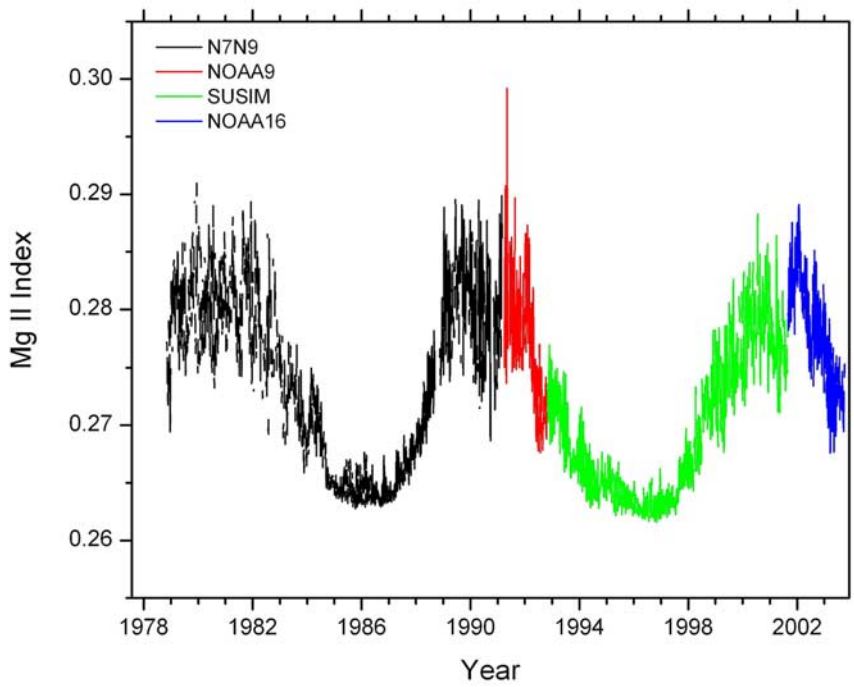

Figure A3. Four primary data sets that make up the overall trends of the Mg II Index.

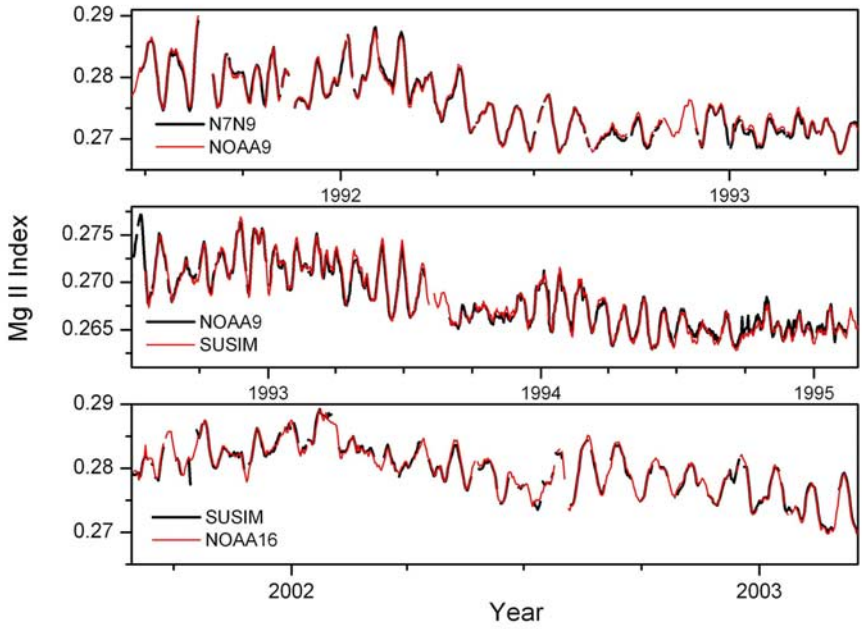

Figure A4. Overlaps between the various data sets. Note that the data sets agree quite well, and it is often difficult to distinguish between the two curves in each plot.

F10.7, but the He I data had so many gaps during the periods of interest that it was not deemed to be useful.

[43] The fitting of the alternate Mg II ratios to the initial time series was accomplished in three steps. First, the secondary data set was selected. When there was more than one data set available to fill a given data gap, the priority for selection of the secondary data set, shown in Table A4, were used. These priorities was established using the scatter and uncertainties in the various data sets.

[44] Once a secondary data set was selected for a given data gap, the secondary data set was scaled to the primary data sets by using 15 data points on each side of the gap. This was done to eliminate small steps at the beginning and end of the data gaps. The missing data were filled with the new data. After a pass through the entire data set, using NOAA 9VP as the secondary data set, the process was repeated using NOAA 16, then NOAA 17, and all the data sets available. In this way 511 of the initial 1372 missing data gaps were filled.

[45] After each pass through the time series, a check for outliers was performed. This process simply removed any single value that deviated by more than 2% from the average of the previous five data points. This level of change was determined to eliminate all of the obvious outliers without removing any reasonably good data.

[46] The remaining 984 missing days were primarily in the first half of the Nimbus 7/NOAA 9 data record when there were no other measurements available. For these missing data points a cubic spline function, based on 18 days on either side of the gap, was used to bridge the gaps of 5 days or less. In tests where existing data were removed to test the splining procedure, the algorithm was able to reproduce the missing data quite accurately (to within 0.5%) for gaps up to 5 days.

[47] Finally, when all of the above techniques had been applied, there were still 121 missing data points. These were all gaps of 5 days or larger. Using the same scaling technique described above, the F10.7 cm solar radio flux was scaled to the Mg II data and used to fill in these larger data gaps. During most of the solar cycle, the F10.7 cm flux was a good approximation for the missing Mg II, but during solar minimum, the fit was not as good. Unfortunately, it was the best data available for the task.

[48] To test the various steps described above, data were removed from the time series and then refitted on the basis of the algorithms described here. The fitted data were compared to the removed data and in all cases the only differences were within the variances of the various data sets.

Table A4. Data Sets and Their Priority in Filling Data Gaps

Priority	Data Set
1	NOAA 9VP
2	NOAA 16
3	NOAA 17
4	SUSIM
5	NOAA 11VP
6	Nimbus 7/NOAA 9
7	GOME
8	NOAA 11DC
9	NOAA 9DC
10	SOLSTICE
11	Spline fit
12	F10.7

References

Allen, M. S., H. C. McAllister, and J. T. Jefferies (1978), High resolution atlas of the solar spectrum 2678-2931 A, 58 pp., Inst. for Astron., Univ. of Hawaii, Honolulu.

Brueckner, G. E., K. L. Edlow, L. E. Floyd, J. L. Lean, and M. E. VanHoosier (1993), The Solar Ultraviolet Spectral Irradiance Monitor (SUSIM) experiment on board the Upper Atmospheric Research Satellite (UARS), *J. Geophys. Res.*, *98*, 10,695–10,711.

Cebula, R. P., and M. T. DeLand (1998), Comparisons of the NOAA-11 SBUV/2, UARS SOLSTICE, and UARS SUSIM Mg II solar activity proxy indexes, *Sol. Phys.*, *177*, 117–132.

Cebula, R. P., M. T. DeLand, and B. M. Schlesinger (1992), Estimates of solar variability using the Solar Backscatter Ultraviolet SBUV2 Mg II index from NOAA-9 satellite, *J. Geophys. Res.*, *97*, 1613–1620.

DeLand, M. T., and R. P. Cebula (1993), Composite Mg II solar activity index for solar cycles 21 and 22, *J. Geophys. Res.*, *98*, 12,809–12,823.

DeLand, M. T., and R. P. Cebula (1994), Comparisons of the Mg II index products from the NOAA-9 and NOAA-11 SBUV/2 instruments, *Sol. Phys.*, *152*, 61–68.

de Toma, G., O. R. White, B. G. Knapp, G. J. Rottman, and T. N. Woods (1997), Mg II core-to-wing index: Comparison of SBUV2 and SOLSTICE time series, *J. Geophys. Res.*, *102*, 2597–2610.

Donnelly, R. F. (1988), The solar UV core-to-wing ratio from the NOAA satellite during the rise of solar cycle 22, *Adv. Space Res.*, *8*, 777–780.

Donnelly, R. F., L. C. Puga, J. Barrett, S. D. Bouwer, J. Pap, D. E. Stevens, and W. K. Tobiska (1994), Solar UV flux measurements from the SBUV2 monitor on the NOAA-9 satellite: Part 1. Mg II *h* and *k* line core-to-wing ratios for 1986–1988, *NOAA Tech. Memo. ERL SEL-85*, 211 pp., Natl. Oceanic and Atmos. Admin., Boulder, Colo.

Floyd, L. E., P. A. Reiser, P. C. Crane, L. C. Herring, D. K. Prinz, and G. E. Brueckner (1998), Solar cycle 22 UV spectral irradiance variability: Current measurements by SUSIM UARS, *Sol. Phys.*, *177*, 79–87.

Frederick, J. E., R. P. Cebula, and D. F. Heath (1986), Instrument characterization for detection of long-term changes in stratospheric ozone: An analysis of the SBUV/2 radiometer, *J. Atmos. Oceanic Technol.*, *3*, 472–480.

Fröhlich, C., and J. Lean (1998), The Sun's total irradiance: Cycles, trends, and related climate change uncertainties since 1976, *Geophys. Res. Lett.*, *25*, 4377–4380.

Hall, L. A., and G. P. Anderson (1988), Instrumental effects on a proposed Mg II index of solar activity, *Ann. Geophys.*, *6*, 531–534.

Heath, D. F., and B. M. Schlesinger (1986), The Mg 280 nm doublet as a monitor of changes in the solar ultraviolet irradiance, *J. Geophys Res.*, *91*, 8672–8682.

Hood, L. L., and S. Zhou (1998), Stratospheric effects of 27-day solar ultraviolet variations: An analysis of UARS MLS ozone and temperature data, *J. Geophys. Res.*, *103*, 3638–3926.

Lean, J. L., G. L. Rottman, H. L. Kyle, T. N. Woods, J. R. Hickey, and L. C. Puga (1997), Detection and parameterization of variations in solar mid- and near-ultraviolet radiation (200–400 nm), *J. Geophys. Res.*, *102*, 29,939–29,956.

Lean, J. L., O. R. White, W. C. Livingston, and J. M. Picone (2001), Variability of a composite chromospheric irradiance index during the 11-year activity cycle and over longer time periods, *J. Geophys. Res.*, *106*, 10,645–10,658.

Pap, J. M., R. C. Willson, C. Frohlich, R. F. Donnelly, and L. Puga (1994), Long-term variations in total solar irradiance, *Sol. Phys.*, *152*, 12–21.

Pap, J. M., A. Vigouroux, and P. Delache (1996), Study of the distribution of daily fluctuations in observed solar irradiances and other full-disk indices of solar activity, *Sol. Phys.*, *167*, 125–143.

Rhoden, E. A., J. M. Forbes, and F. A. Marcos (2000), The influence of geomagnetic and solar variabilities on lower thermospheric density, *J. Atmos. Sol. Terr. Phys.*, *62*, 999–1013.

Rottman, G. J., T. N. Woods, and T. P. Sparn (1993), Solar Stellar Irradiance Comparison Experiment 1: 1. Instrument design and operation, *J. Geophys. Res.*, *98*, 10,667–10,678.

Thuillier, G., and S. Bruinsma (2001), The Mg II index for upper atmosphere modeling, *Ann. Geophys.*, *19*, 219–228.

Tobiska, W. K., T. Woods, F. Eparvier, R. Viereck, L. Floyd, D. Bouwer, G. Rottman, and O. R. White (2000), The SOLAR2000 empirical solar irradiance model and forecast tool, *J. Atmos. Sol. Terr. Phys.*, *62*, 1233–1250.

Viereck, R. A., and L. C. Puga (1999), The NOAA Mg II core-to-wing solar index: Construction of a 20-year times series of chromospheric variability from multiple satellites, *J. Geophys. Res.*, *104*, 9995–10,005.

Viereck, R. A., L. Puga, D. McMullin, D. Judge, M. Weber, and W. K. Tobiska (2001), The Mg II index: A proxy for solar EUV, *Geophys. Res. Lett.*, *28*(7), 1343–1346.

Weber, M., J. P. Burrows, and R. P. Cebula (1998), GOME solar irradiance measurements between 1995 and 1997: First results on proxy solar activity studies, *Sol. Phys.*, *177*, 63–77.

White, O. R., G. de Toma, G. J. Rottman, T. N. Woods, and B. G. Knapp (1998), Effects of spectral resolution on the Mg II index as a measure of solar variability, *Sol. Phys.*, *177*, 89–103.

Wilson, R. C. (1997), Total solar irradiance trend during solar cycles 21 and 22, *Science*, *277*(5334), 1963–1965.

Woods, T. N., G. J. Rottman, and G. J. Ucker (1993), Solar Stellar Irradiance Comparison Experiment 1: 2. Instrument calibrations, *J. Geophys. Res.*, *98*, 10,679–10,694.

P. C. Crane, Remote Sensing Division, Code 7213, Naval Research Laboratory, 4555 Overlook Avenue, SW, Washington, DC 20375, USA. (patrick.crane@nrl.navy.mil)

M. T. DeLand, Science Systems and Applications Inc, 10210 Greenbelt Rd., Suite 400, Lanham, MD 20706, USA. (matthew_deland@ssaihq.com)

L. E. Floyd, Interferometrics, Inc., 14120 Parke Long Court #113, Chantilly, VA 20151-1646, USA. (linton.floyd@nrl.navy.mil)

B. G. Knapp, G. Rottman, and T. N. Woods, Laboratory for Atmospheric and Space Physics, University of Colorado, 1234 Innovation Drive, Boulder, CO 80303, USA. (barry.knapp@lasp.colorado.edu; gary.rottman@lasp.colorado.edu; tom.woods@lasp.colorado.edu)

L. C. Puga and R. A. Viereck, NOAA SEC, 325 Broadway, Boulder, CO 80305-3328, USA. (laurence.puga@noaa.gov; rodney.viereck@noaa.gov)

M. Weber, Institute of Environmental Physics, University of Bremen, PO Box 330 440, D-28334 Bremen, Germany. (weber@uni-bremen.de)